Cell, Vol. 95, 939–950, December 23, 1998, Copyright ©1998 by Cell Press

Crystal Structure of Constitutive Endothelial Nitric Oxide Synthase: A Paradigm for Pterin Function Involving a Novel Metal Center

C. S. Raman,*‖ Huiying Li,*‖ Pavel Martásek,† Vladimir Král,‡ Bettie Sue S. Masters,†§ and Thomas L. Poulos*§

*Department of Molecular Biology and Biochemistry
University of California
Irvine, California 92697-3900

†Department of Biochemistry
University of Texas Health Science Center
San Antonio, Texas 78284-7760

‡Department of Analytical Chemistry
Institute of Chemical Technology
Prague 6
Czech Republic

Summary

Nitric oxide, a key signaling molecule, is produced by a family of enzymes collectively called nitric oxide synthases (NOS). Here, we report the crystal structure of the heme domain of endothelial NOS in tetrahydrobiopterin (H_4B)-free and -bound forms at 1.95 Å and 1.9 Å resolution, respectively. In both structures a zinc ion is tetrahedrally coordinated to pairs of symmetry-related cysteine residues at the dimer interface. The phylogenetically conserved Cys-$(X)_4$-Cys motif and its strategic location establish a structural role for the metal center in maintaining the integrity of the H_4B-binding site. The unexpected recognition of the substrate, L-arginine, at the H_4B site indicates that this site is poised to stabilize a positively charged pterin ring and suggests a model involving a cationic pterin radical in the catalytic cycle.

Introduction

Nitric oxide (NO), a free radical, is a ubiquitous signaling molecule that participates in diverse cellular processes, including regulation of blood pressure, neurotransmission, and the immune response (Dinerman et al., 1993). NO is produced by nitric oxide synthases (NOS), which consist of a heme domain linked via a calmodulin binding linker peptide to a NADPH-cytochrome P450 reductase-like diflavin domain, resulting in a large polypeptide (Mr 130,000–160,000). Only dimeric NOS is catalytically active. Upon Ca^{2+}/calmodulin binding, the FAD of the flavoprotein domain transfers reducing equivalents from NADPH to FMN, which then reduces the heme iron. Reduction of the heme iron leads to O_2 activation followed by oxidation of an L-Arg guanidino N atom to NO and L-citrulline (Marletta, 1994).

NOS constitute a family of enzymes of which three genetically encoded isoforms have been identified in mammalian systems (Knowles and Moncada, 1994; Griffith and Stuehr, 1995; Masters et al., 1996). The neuronal (nNOS) and endothelial NOS (eNOS) are constitutive with posttranslational regulation of enzyme activity. The inducible isoform (iNOS) is produced in response to certain stimuli (e.g., cytokines) and is regulated mostly at the level of transcription (Nathan, 1995). Under normal conditions, NO mediates the regulation of blood pressure in healthy human subjects and cerebral blood flow associated with neuronal activation. Uncontrolled generation of NO, however, can lead to pathology. While overproduction of NO by nNOS and iNOS is directly linked to the pathogenesis of stroke (Huang et al., 1994) and shock (Nathan, 1995), respectively, NO generated by eNOS has been shown to be antiatherogenic and critical for angiogenesis. Therefore, isoform-specific drugs are required to inhibit NO production by nNOS and iNOS under pathological conditions without hindering NO generation by eNOS. In addition, upregulation of eNOS via suitable activators holds a significant therapeutic potential in controlling cardio- and cerebrovascular disorders.

Both iNOS and nNOS are cytosolic enzymes, while eNOS is membrane bound (Pollock et al., 1991). eNOS also is unique in that it is targeted to the caveolae (Shaul et al., 1996) of vascular endothelial cells, where it is dynamically regulated by interactions with caveolin (García-Cardeña et al., 1997). All three NOS isoforms exhibit an absolute requirement for (1'R, 2'S, 6R)-5,6,7,8-tetrahydrobiopterin (H_4B) as a cofactor to function (Kwon et al., 1989; Tayeh and Marletta, 1989; Kaufman, 1997), and only reduced pterin can sustain catalysis. Despite extensive biochemical studies, the role of pterin function in NOS remains a mystery (Hemmens and Mayer, 1997). Under conditions of reduced H_4B availability, there is strong evidence for superoxide generation by eNOS (Vásquez-Vivar et al., 1998) leading to potential pathophysiology. Furthermore, endothelial dysfunction is reversed in hypercholesterolemic patients treated with H_4B and has been shown to be a NOS-related action (Stroes et al., 1997). The availability of pterin-free structure can shed light on the molecular basis of superoxide generation by dysfunctional eNOS in H_4B-depleted states.

Recently, Crane et al. have reported the crystal structures of the iNOS oxygenase domain monomer (1997) and H_4B-bound dimer (1998). The iNOS monomer is both catalytically inactive and unable to bind either the substrate or H_4B (Ghosh et al., 1997). Only the dimer is physiologically relevant and retains the ability to bind substrate and cofactor, H_4B. Crane et al. (1998) have compared the crystal structures of the inactive iNOS monomer and the H_4B-bound dimer and conclude that pterin binding (a) is critical for dimer formation; (b) results in major conformational changes; (c) creates both the active-center channel and L-Arg-binding site; and (d) leads to the formation of both reductase and caveolin-binding sites. Here, we have addressed pterin function in NOS by determining the high-resolution crystal structure of the dimeric eNOS heme domain both alone and in complex with H_4B. By a direct comparison of the dimeric pterin-free and -bound eNOS heme domain structures we show that pterin binding (1) is not

§To whom correspondence should be addressed (e-mail: poulos@uci.edu [T. L. P.], masters@uthscsa.edu [B. S. S. M.]).

‖These authors contributed equally to this work.

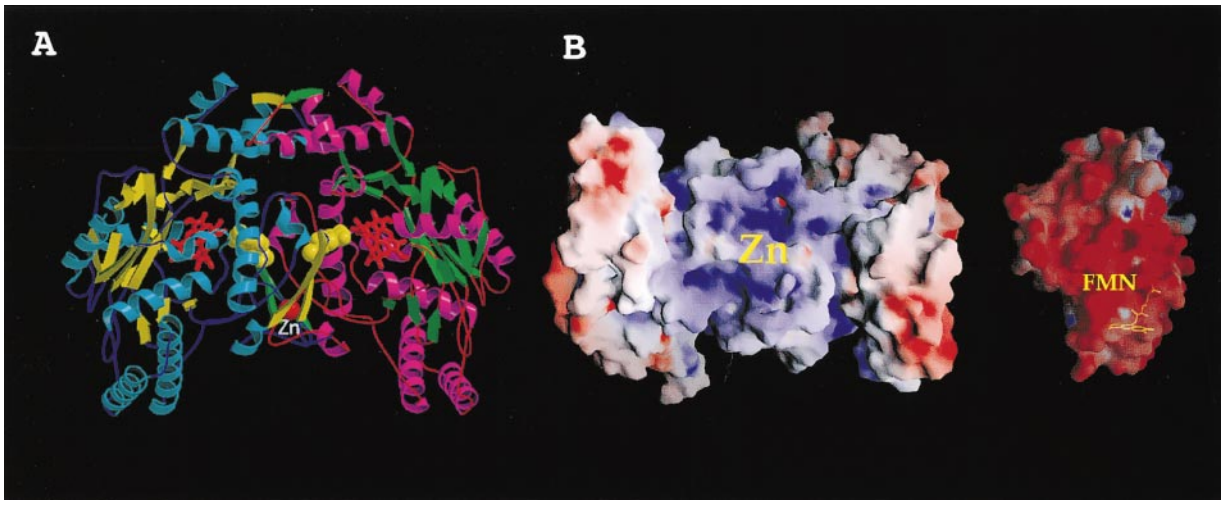

Figure 1. Tertiary Topology, Quaternary Structure, and Docking Surface of eNOS Heme Domain

(A) Ribbon diagram of the eNOS heme domain dimer (+H_4B, +SEITU data). The two H_4B molecules are shown as yellow space-filled models. The zinc located along the dyad axis of symmetry is highlighted as a red sphere. (B) Molecular surface map of the electrostatic potential of the eNOS heme domain dimer calculated using GRASP (Nicholls et al., 1993). The blue and red contours represent positive and negative potential (full saturation = 16 kT), respectively. This view is rotated 90° from the orientation shown in (A) such that the viewer is looking toward the ZnS_4 center directly along the two-fold relating the monomers. The complementary electrostatic surface potential of the eNOS heme domain and the FMN domain of the P450 reductase (Wang et al., 1997) depicts the proposed docking site between the two proteins.

required for dimer formation, (2) fails to produce conformational changes either at the H_4B site or anywhere else in the protein, (3) neither affects substrate, L-Arg, binding, nor is required for the creation of the active site/channel, and (4) does not elicit structural changes at the proposed reductase and caveolin interaction sites. Further, Crane et al. (1998) identified a disulfide bridge at the bottom of the dimer interface involving a pair of cysteine residues, one from each monomer. We unambiguously establish that these evolutionarily conserved cysteines are involved in coordinating a zinc atom that functions both to stabilize the H_4B-binding site and to facilitate stereospecific pterin recognition.

Here, we present a high-resolution crystal structure of a constitutive NOS (eNOS) heme domain both alone and in complex with H_4B. The similarity between the pterin-binding site in NOS and other pterin-utilizing enzymes indicates a catalytic role for H_4B. We also provide structural evidence for the ability of the substrate, L-Arg, to bind at the H_4B site. The cofactor mimicry by the substrate suggests a mechanism that directly implicates the participation of a pterin radical cation in the catalytic cycle leading to NO biosynthesis. Further, the pterin-free dimer structure provides a molecular proving ground for understanding the dysfunctional eNOS generated in H_4B-depleted pathological states.

Results and Discussion

Structure and Conformation of the eNOS Heme Domain

The eNOS heme domain (Figure 1) belongs to the α/β protein class, and the quaternary structure is characterized by a tightly packed dimer interface that buries 3000 $Å^2$ (per subunit) of solvent-accessible surface (55% hydrophobic and 45% polar). The overall fold of the eNOS heme domain dimer is similar to that reported for the lower resolution (2.6 Å) mouse iNOS dimer structure (Crane et al., 1998). A novel feature of the eNOS structure that was not observed in the iNOS structure is the presence of a Zn ion tetrahedrally coordinated to pairs of symmetry-related Cys residues (Figures 1 and 2). Crane et al. (1998) interpreted this region in iNOS as an intersubunit disulfide bond between symmetry-related Cys-109 residues that correspond to one of the ligands in eNOS, Cys-101. They also noted a disordering in residues 101–107 immediately preceding Cys-109. This apparent discrepancy between the two structures could be explained by a comparison of the proteins used in structure determination. Crane et al. (1998) obtained the iNOS oxygenase domain by independently expressing it in *Escherichia coli*, whereas the eNOS heme domain used in this study was derived via trypsinolysis of the holoenzyme (containing both heme and reductase domains in a single polypeptide chain). NOS heme domains expressed per se have a tendency not to incorporate the metal ion (R. T. Miller and B. S. S. M., unpublished data). In the absence of the metal, due to the close structural proximity of the sulfhydryls, a disulfide bond can form in vitro. However, considering the strongly reducing conditions in the cytosol, the formation of a disulfide would be both kinetically and thermodynamically disfavored (Schwabe and Klug, 1994). Hence, the loss of zinc in the iNOS structure most likely led to the disordering of the polypeptide chain in this region. Owing to the strict conservation of the Cys-$(X)_4$-Cys motif (Figure 3) in all NOS sequences known to date, the zinc center is expected to be a common feature of all NO synthases.

Role of ZnS_4 in Pterin Binding and Reductase Docking

The zinc tetrathiolate, ZnS_4 or $(Zn[S\text{-cysteine}]_4)^{2-}$, metal center in eNOS is located at the bottom of the dimer

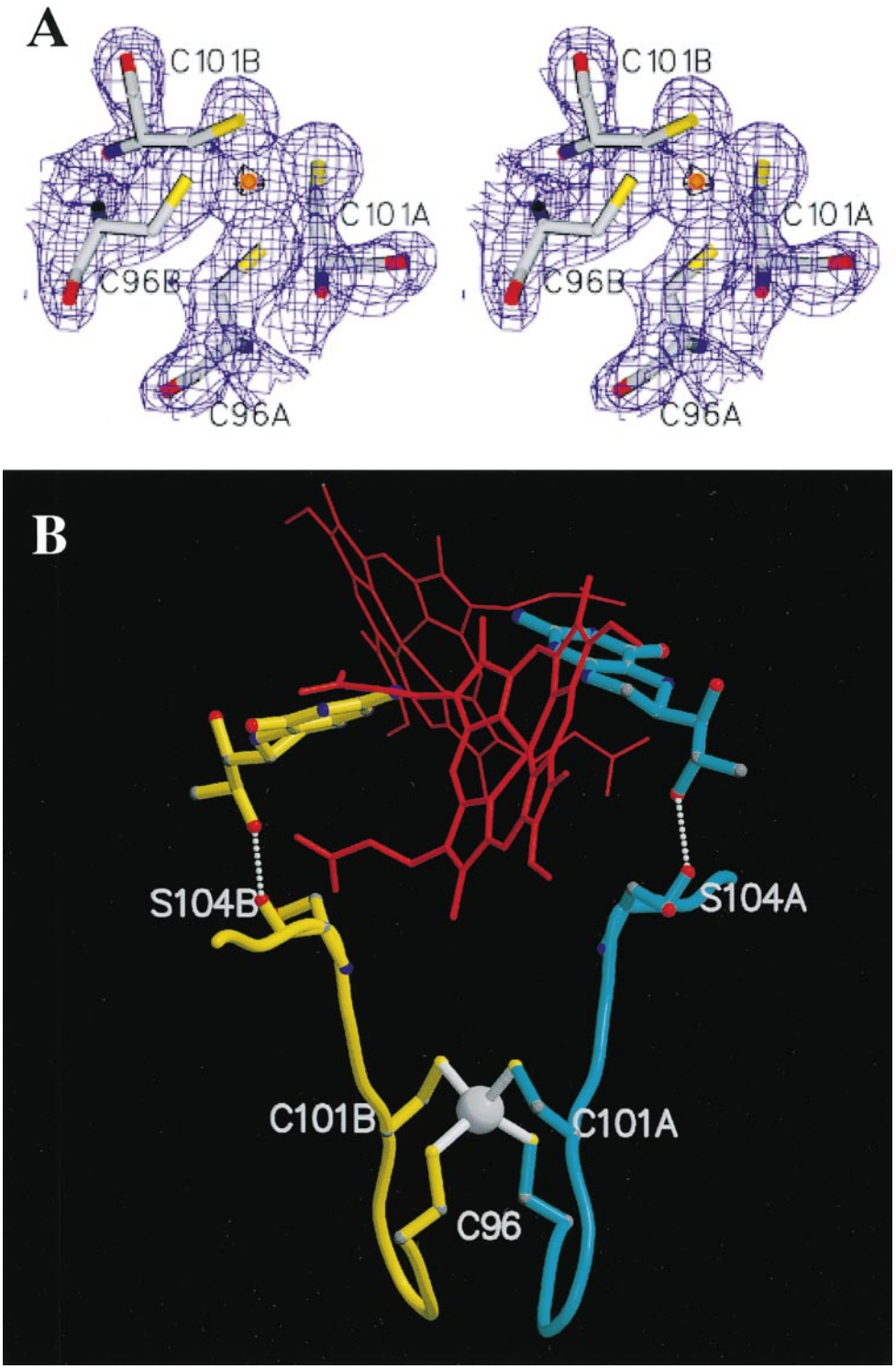

Figure 2. ZnS_4 Center at the Dimer Interface of eNOS Heme Domain

(A) Stereo view of the $2F_o-F_c$ 1.9 Å omit electron density map around the zinc metal center ($+H_4B$, +SEITU data). The map was obtained from model phases after a round of simulated annealing with the atoms shown excluded from the refinement. The map is contoured at 1 σ (blue) and 10 σ (black). The zinc ion was identified using anomalous dispersion effects characteristics for the metal. X-ray wavelengths of 1.280 Å and 1.286 Å (zinc absorption edge, λ = 1.283 Å) were chosen using a tunable synchrotron X-ray source. Zinc exhibits significant anomalous scattering effects at 1.280 Å with little anomalous scattering contribution at 1.286 Å. Heme Fe exhibits some anomalous scattering at both wavelengths (iron absorption edge, λ = 1.739 Å). Direct methods (Sheldrick, 1997) also were used to independently identify the anomalous scatterers.

(B) The ZnS_4 metal center and its relationship to H_4B. Ser-104 is part of the loop containing the cysteine ligands and H-bonds to the C6 side chain of pterin. The stereospecific recognition of H_4B by NOS is dictated by the substitution at the C6 position.

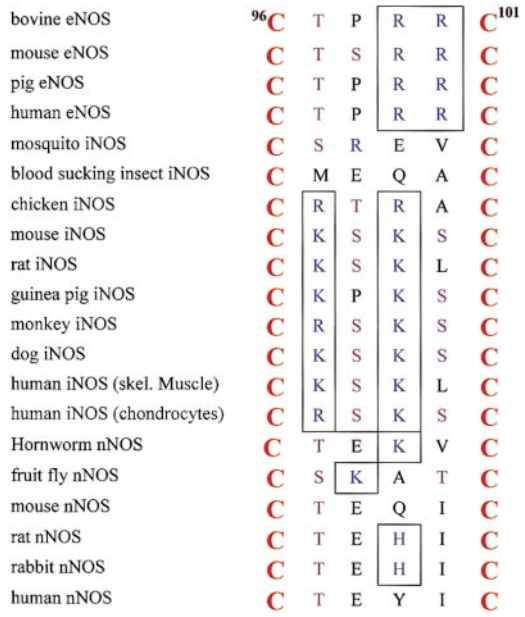

Figure 3. Sequence Alignments Depicting the Zinc-Binding Motif in NOS

The strict conservation of the cysteine ligands in NOS utilized in coordinating the zinc atom are shown. Within the Cys-$(X)_4$-Cys motif, -$(X)_4$- exhibits a preferential bias toward hydroxylated (Ser and Thr) and charged (Arg, His, and Lys) residues.

interface (Figure 1A) with the metal tetrahedrally coordinated by two pairs of symmetry-related cysteine residues (Figure 2, Cys-96 and Cys-101) from each subunit. The cysteine ligands are part of a small three-stranded antiparallel β sheet (two strands from one monomer and one strand from the other) that orients Cys-96 and Cys-101 in the same direction directly across antiparallel strands. In addition to the β strand main chain H-bonds, Sγ (96) and Sγ (101) form H-bonds with the peptide NH residues Leu-102 and Gly-103, respectively. Also, the amide N of Cys-101 is H-bonded to the >C=O of Asn-468. This H-bonding pattern differs from that observed in the rubredoxin "knuckle-motif" (Cys-$(X)_2$-Cys) (Schwabe and Klug, 1994), where each cysteine side chain Sγ (i) forms an H-bond with the backbone amide of the i + 2 residue. However, the extensive H-bond network is in large part due to the formal negative charge on the sulfur ligands. H-bonds between sulfur ligands and amide NH groups are a signature of metal sulfur centers.

The zinc is positioned equidistant from each heme (21.6 Å) and H_4B (12 Å) with one of its ligands, Cys-101, separated only by two residues from Ser-104, which H-bonds directly to the pterin side chain hydroxyl (Figure 2B). In addition, Val-106 forms a direct nonbonded contact with H_4B. Therefore, disruption of the metal center either by demetallation or ligand removal via mutagenesis will distort this region of the polypeptide chain resulting in diminished affinity for H_4B. Since H_4B couples directly to the heme, alterations at the pterin site will in turn affect the heme pocket and L-Arg binding. These structural findings help explain why a large body of mutational data shows dramatic loss in protein stability, catalytic activity, and H_4B binding upon removal of the zinc ligands in NOS (Chen et al., 1995; Ghosh et al., 1997; Miller et al., 1997; Rodríguez-Crespo et al., 1997).

ZnS_4 centers have been observed in only four other enzymes (Vallee and Auld, 1993; Lipscomb and Sträter, 1996), including cytochrome oxidase (Tsukihara et al., 1995) and *Bacillus stearothermophilus* adenylate kinase (Berry and Phillips, 1998), where they play a structural role. eNOS presents a unique scenario in which the ZnS_4 center is sandwiched at the dimer interface in the vicinity of the pterin-binding site. The metal center acts in a structural capacity by helping to maintain the integrity of the pterin-binding site. Furthermore, the most extensive electropositive region on eNOS surrounds the ZnS_4 center (Figure 1B). This surface can provide an excellent docking site for the strongly electronegative reductase domain. This would also enable the electron donor (FMN domain) to be in spatial proximity to the ZnS_4 center. The apparent requirement of the reductase domain for the proper insertion of the metal center, as demonstrated by the derivation of the heme domain dimer from the holoenzyme constructs in these studies, argues in favor of the close proximity between the ZnS_4 and the reductase domain. Both the zinc atom and its ligands are accessible to solvent in the heme domain structure and could have limited access in the holo-protein in which the FMN domain would be docked in the metal center's vicinity. Interestingly, both Mss4 (Yu and Schreiber, 1996) and LIM (Schmeichel and Beckerle, 1994) proteins utilize ZnS_4-containing surfaces to mediate protein–protein interactions, and a similar function could be envisioned for the metal center in NOS enzymes as well.

Crane et al. (1998) proposed a docking site that includes Trp-366 of iNOS oxygenase domain for interaction with the reductase and caveolin-1. They also suggest that this region undergoes a conformational change upon pterin binding to facilitate docking. Since eNOS, and not iNOS, is targeted to the caveolae (Shaul et al., 1996), it was of interest to examine this site for its ability to dock with caveolin (García-Cardeña et al., 1997). The proposed recognition motif for caveolin-1 in eNOS, Phe-$(X)_4$-Phe-$(X)_2$-Trp (Couet et al., 1997), is primarily solvent inaccessible (using a 1.4 Å probe) exposing only the indole ring of the terminal Trp-358. In addition, since neither pterin-free nor -bound structures show any difference in this region, the ability of the proposed region to support caveolin and reductase recognition is suspect.

The identification of ZnS_4 in eNOS has physiological relevance. If one or more cysteine ligands could remain nucleophilic, it would be possible for the cysteine ligand(s) to undergo S-nitrosylation (Stamler, 1994) followed by the ejection of zinc. The DNA repair enzyme, *Escherichia coli* Ada, provides a known example where the nucleophilicity of the cysteine coordinated to zinc (ZnS_4) is preserved (Wilker and Lippard, 1995) and utilized in catalysis. The release of zinc may also be controlled by the redox status in situ (Maret and Vallee, 1998). NO can release zinc from ZnS_4 clusters of proteins (Gergel and Cederbaum, 1996), including transcription factors and NOS (R. T. Miller and B. S. S. M., unpublished observations), and it remains to be established whether nitrosative stress in vivo can regulate NO biosynthesis.

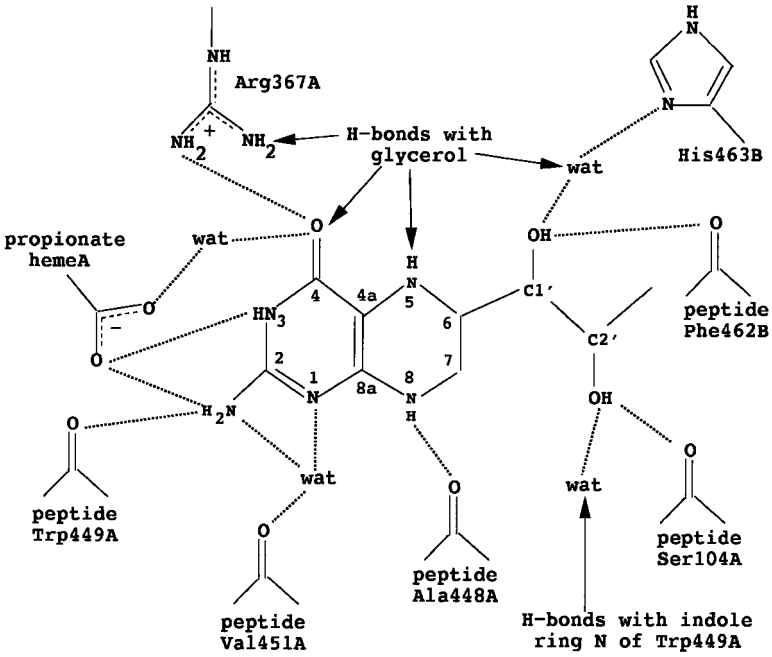

Figure 4. Hydrogen Bond Networks at the H_4B-Binding Site

Given the zinc requirement for endothelial function, it is conceivable that acquired vascular dysfunction can be associated with mutations that weaken zinc affinity resulting in dysfunctional eNOS. While no such mutations are known at present, a parallel can be drawn from familial amyotropic lateral sclerosis, in which over 50 independent variants in Cu/Zn-superoxide dismutase give rise to a common toxic phenotype invariably characterized by decreased zinc affinity (up to 100,000-fold; Crow et al., 1997).

Structural Determinants for H_4B Binding and Its Relationship to the Pterin Family of Enzymes

The high-resolution structure of the pterin-bound eNOS heme domain facilitates not only a quantitative analysis of the H_4B–protein interactions, but also addresses the stereospecificity of cofactor recognition via the newly identified ZnS_4 center. The extensive H-bond network involving pterin and eNOS (Figure 4) attests to the cofactor's unusually high affinity (K_d 20 nM; Werner-Felmayer and Gross, 1996). NOS enzymes have a preference for the fully reduced (R) stereoisomer of H_4B with the (S) isomer binding weakly and less effective in sustaining catalysis (Presta et al., 1998). The H-bond network in eNOS aids in understanding the structural basis for the favored chiral centers at C6, C1', and C2' of H_4B (Figure 4). The molecular recognition of H_4B is mediated by one of the heme propionate groups in which a carboxylate oxygen H-bonds directly with the pyrimadone moiety (N-3 and the amine at C-2) of the pterin. The same propionate is also H-bonded to the amino group of the substrate L-Arg. The other carboxylate oxygen establishes a water-bridged H-bond with the 4-keto group. Arg-367 also makes a direct H-bond to this group. Another key interaction in H_4B recognition involves Ser-104, which H-bonds to the dihydroxypropyl side chain and helps orient it. The strategic location of Ser-104, as part of a loop involved in zinc ligation (Figure 2B), emphasizes the importance of the zinc center in ensuring stereospecific recognition of H_4B.

A comparison of the H_4B binding mode in eNOS with other enzymes that either utilize pterin as a substrate or cofactor reveals insights into pterin function in NO biosynthesis. First, the recognition of the H_4B pyrimadone by the heme propionate in eNOS is comparable to the use of Asp or Glu residues by other pterin enzymes. For example, an acidic residue always forms bifurcated H-bonds via its carboxylate function with the N-2 and N-3 nitrogens of the pterin substrate (Auerbach et al., 1997). In addition, dihydrofolate reductase (DHFR; McTigue et al., 1993), dihydroneopterin aldolase (Hennig et al., 1998), dihydropteroate synthase (DHPS; Hampele et al., 1997), thymidylate synthase (TS; Birdsall et al., 1996), and the molybdopterin oxidoreductase (Chan et al., 1995) all utilize a carboxylate to interact with the pterin. Second, the pterin recognition in NOS is reminiscent of the GTP-binding motif of the GTPase superfamily of proteins, which provide an archetypal protein carboxylate for interacting with the pyrimadone moiety (Bourne et al., 1991). Thus, NOS has evolved to retain a carboxylate for mediating pterin recognition, but unlike the GTPase superfamily, it utilizes a propionate of the heme prosthetic group. Third, the aromatic stacking of the pterin in eNOS (Figures 4 and 5A) is surprisingly similar to that seen in the ricin–neopterin complex (Yan et al., 1997) and in TS (Birdsall et al., 1996).

While the similarities between H_4B recognition in NOS and other pterin-utilizing enzymes are striking, the differences provide clues to why NO biosynthesis requires pterin as a cofactor. Only in NOS, DHPS, and ricin is a positively charged residue positioned within H-bonding distance to the 4-keto group of the pteridine ring. In all other cases a main chain amide acts as the H-bond donor. Pteridine dehydratase (DCoH; Cronk et al., 1996), tyrosine hydroxylase (TyrOH; Goodwill et al., 1998), and

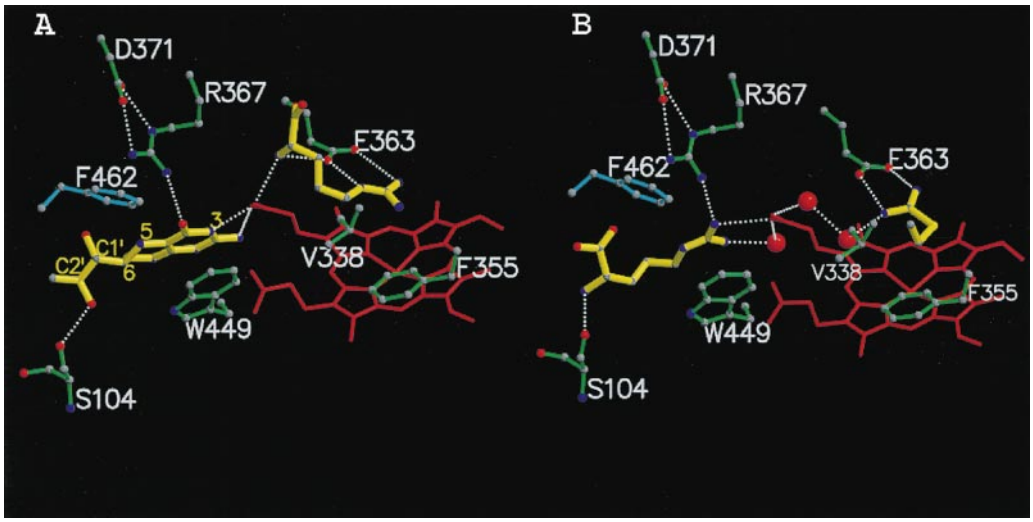

Figure 5. Cooperativity and Molecular Mimicry in eNOS

(A) Cross talk between H_4B and L-Arg mediated by the heme propionate (Se-edge data). The guanidinium and amino groups of L-Arg are held in place by H-bonding with the conserved Glu-363. The amino group also H-bonds with a heme propionate. H_4B H-bonds directly with the heme propionate, while the pteridine ring is sandwiched between Phe-462 in one monomer and Trp-449 in another, respectively.

(B) L-Arg is a structural mimic of H_4B at the pterin-binding site when SEITU is bound at the active site (-H_4B, +SEITU data). L-Arg binds to the pterin site and exquisitely mimics the H_4B interaction with eNOS ([A] and Figure 4). The specific interaction of the potent inhibitor, SEITU, at the active site is mediated by a pair of bifurcated H-bonds to Glu-363. Two water molecules bridge between the inhibitor and heme propionate. The ethyl group of the inhibitor forms nonbonded contacts with Val-338 and Phe-355. The ureido sulfur is positioned 3.5 Å and 4.0 Å above heme pyrrole B-ring nitrogen and the heme iron, respectively.

dihydropteridine reductase (DHPR; Varughese et al., 1992) incorporate the most significant differences in pterin recognition when compared to NOS and other pterin enzymes. In sharp contrast to eNOS, neither TyrOH nor DCoH, which use H_4B as a cofactor and substrate, respectively, involves direct protein interaction with N-3 of the pterin. This is because the catalytic step in both enzymes involves oxidation/reduction at the pyrimidine portion of the pterin ring. qH_2B recognition by DHPR appears to adopt a similar mode of interaction as well (Varughese et al., 1992). The pterin-binding site in TyrOH and DHPR also is accessible to solvent such that the product can be easily released toward regeneration of the substrate. In NOS, H_4B is tied down by numerous H-bonded and water-bridged interactions to prevent facile release into the solvent (Figure 4). This is in excellent agreement with the three orders of magnitude (Werner-Felmayer and Gross, 1996) greater affinity for H_4B of NOS compared to TyrOH. Furthermore, a tightly held glycerol molecule occupies the space above the 4a position of H_4B in eNOS. Glycerol is a leftover from protein purification. In its absence, solvent molecules are expected to fill this region. Perry and Marletta (1998) recently suggested that NOS resembles the aromatic amino acid hydroxylases (AAH) with respect to pterin function. Unlike the TyrOH case (Goodwill et al., 1998), a non–heme iron center, which directly participates in catalysis, is absent within a 5.6 Å distance of the 4a position of H_4B in eNOS. This region in eNOS is also devoid of multiple ligands to sustain metal ligation. In addition, cocrystallization in the presence of $FeSO_4$ (10 mM) failed to reveal metal binding (via anomalous scattering) in the vicinity of the 4a position of H_4B. Thus, the mechanism of pterin function in NOS has no discernible similarities to TyrOH, DCoH, or DHPR.

Three major conclusions stem from the structural dissection of the pterin site in eNOS. First, $H_4B \leftrightarrow qH_2B$ cycling, observed in AAH catalysis, can be ruled out in NOS, since the highly activated pyrimidine nucleus of H_4B is adequately protected by H-bonds. In addition, the non–heme iron center, a sine qua non for catalysis in AAH, is absent in eNOS. These observations provide a structural basis for understanding why oxidation products of pterin have not been observed during NOS catalysis (Tayeh and Marletta, 1989). In this regard, NOS resembles enzymes that utilize tetrahydrofolate as cofactors without taking advantage of redox properties of the H_4B ring system (Matthews, 1982). Second, an inherent DHPR-like activity (Witteveen et al., 1996) can also be ruled out since structural comparisons between the pterin site in eNOS and DHPR (Varughese et al., 1992) fail to reveal similarities. Third, the H_4B-binding site of eNOS strongly resembles the catalytic site of enzymes that utilize pterin as a substrate. Thus, H_4B directly participates in catalysis and undergoes a chemical rearrangement unlike either AAH or pteridine reductase.

Pterin-Free Structure, Molecular Mimicry, and Structural Basis for H_4B Substrate Cooperativity

There is an ongoing debate regarding the function of pterin in NOS structure and catalysis (Hyun et al., 1995; Hemmens and Mayer, 1997; Perry and Marletta, 1998). Recently, Crane et al. (1998) compared the structure of an inactive iNOS oxygenase domain monomer with a H_4B-bound dimer structure. They concluded that pterin binding was critical for dimer formation. They further suggested that pterin binding results in a major conformational change leading to active site/channel

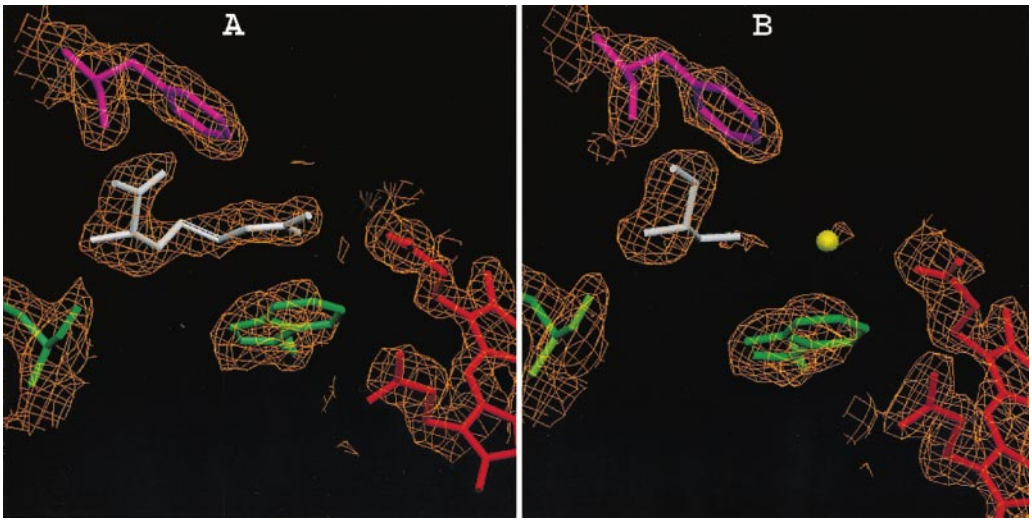

Figure 6. Pterin-Free Structures of eNOS

(A) $2F_o-F_c$ 2.1 Å omit electron density map showing L-Arg bound at the pterin-binding site (-H_4B, +SEITU data).

(B) $2F_o-F_c$ 1.95 Å omit electron density map illustrating the empty pterin-binding site occupied only by solvent molecules (-H_4B, +Arg data). A glycerol molecule has been modeled to account for the residual density.

formation and controls the generation of the reductase and caveolin docking sites. It is important to note, however, that the iNOS monomer used in the crystal structure work (Crane et al., 1997) was missing the first 114 residues essential for dimerization and zinc binding. The iNOS monomer is also catalytically incompetent due to its inability to bind both substrate and cofactor (Ghosh et al., 1997). As a result, functionally important comparisons between the iNOS monomer and dimer structures cannot be made. In an effort to identify the true function of pterin in NOS structure and catalysis, we have solved the structure of eNOS heme domain dimer, both in the H_4B-free and -bound states. The eNOS protein used in this study was obtained via expression in *Escherichia coli*, which inherently lacks the machinery to synthesize H_4B. The protein is dimeric (Martásek et al., 1996; Venema et al., 1997) even in the total absence of pterin and retains the ability to readily bind substrate and H_4B.

In the absence of H_4B, the overall eNOS heme domain structure remains unchanged both in tertiary topology and quaternary structure. Comparison of the pterin-bound (Figure 5A) and -free (Figure 6B) structures reveals that the H_4B site preexists in eNOS. Furthermore, it is possible to soak H_4B into pterin-free eNOS heme domain crystals without disturbing the crystal lattice. Both the substrate channel and the active site are unaffected by the lack of pterin at the H_4B-binding site. In fact, the mode of L-Arg binding at the active site in the pterin-free structure of eNOS is identical to that seen in the H_4B-bound structure (data not shown). There also is biochemical evidence for substrate analog (N^{ω}-nitro-L-arginine) recognition by eNOS even in the absence of H_4B (Martásek et al., 1996). The neuronal (Roman et al., 1995) isoform, however, shows a strict prerequisite for H_4B to facilitate N^{ω}-nitro-L-arginine binding. Since the heme propionate is a common denominator for both substrate and H_4B recognition (Figure 5A), the cooperativity between the two sites may be mediated by stringent positioning of the heme propionate. Thus, both the pterin and active sites preexist and do not form via conformational changes or induced fit resulting from ligand binding, as suggested by Crane et al. (1998).

The 1.95 Å pterin-free structure (Figure 6B) also holds clues to explain why under conditions of limited H_4B availability, eNOS and, in particular, the heme domain produce the deleterious superoxide radical (Vásquez-Vivar et al., 1998). This is of considerable physiologic interest since H_4B depletion is associated with vascular pathology (Cosentino et al., 1998). Supplementation with H_4B, however, totally couples L-Arg oxidation to NO synthesis, and superoxide generation is prevented. Since there are no major structural changes at the active or H_4B sites in pterin-free eNOS (rmsd $<$ 0.3 Å), lack of occupancy at the pterin site with precise orientational constraints must be the basis for superoxide production. The substrate is able to bind in the absence of pterin, but it is unable to prevent superoxide production, thus implicating H_4B in controlling the latter. The uncoupling of L-Arg oxidation to NADPH consumption due to the lack of H_4B probably leads to electron transfer to molecular oxygen, resulting in superoxide production. The eNOS–H_4B interaction is reminiscent of the need for proper positioning of the flavin isoalloxazine cofactor, during turnover, for total coupling in the catalysis of p-hydroxybenzoate hydroxylase (Gatti et al., 1994).

The pterin-free eNOS structure with a potent inhibitor, S-ethylisothiourea (SEITU; K_d 30 nM, Garvey et al., 1994), bound at the substrate site (Figure 5B), reveals a surprising result. The pterin site is no longer empty and is now occupied by the substrate, L-arginine. The mode of L–Arg interaction at the pterin site (Figures 5B and 6A) mimics that entertained by H_4B itself (Figure 5A). Two critical H-bonds with L-arginine, one between a guanidino N and the heme propionate, and another involving the primary amino group and Ser-104 are strictly conserved (Figure 6A). Moreover, the planar guanidinium group is sandwiched between two aromatic groups, one from each monomer, exactly as in the H_4B

complex. The affinity for L-Arg must be significant, since no exogenous L-Arg was added during crystallization and only 200 μM of the substrate was carried over from protein purification. The specificity of L-Arg recognition at the pterin site appears to require both the guanidino function and the primary amino group since SEITU (5 mM used in cocrystallization) was unable to displace L-Arg from the pterin site. The existence of cooperativity between the substrate and H_4B sites is further highlighted by the discovery that L-Arg can occupy the pterin site when a strong inhibitor is bound at the active site. It is puzzling that L-Arg occupies the pterin site only when SEITU is bound at the active site and not when the substrate occupies the latter site. Alderton et al. (1998) have provided empirical evidence for the ability of SEITU to promote pterin binding. Thus, the inhibitor-bound conformation may facilitate L-Arg binding at the pterin site, owing to the strong structural similarity between the substrate and pterin.

It is conceivable that the H_4B site possibly evolved from what was originally an L-Arg-binding site and may provide clues toward understanding the primordial NOS catalytic machinery. Furthermore, the higher affinity of NOS for H_4B may have evolved to repel competition from L-Arg, which is abundant in cells (0.2–0.8 mM; Hecker et al., 1992). A striking corollary can be established between our finding and the ability of *Tetrahymena* group I catalytic RNA to specifically recognize L-Arg as a competitive inhibitor and mimic for guanosine binding (Yarus 1988).

Implications for the Role of Pterin Radical in NOS Catalysis

The elegant mimicry of the obligatory H_4B cofactor by L-Arg provides mechanistic insights into the role played by pterin in NOS catalysis. The specific recognition of L-Arg at the H_4B site (Figure 6A) in eNOS suggests the ability of this site to stabilize a positively charged state of the pterin ring and, particularly, the pterin cation radical (Figure 7). In order for NOS to utilize a pterin radical, extensive protonation of the bound H_4B is necessary. L-Arg binding to the pterin site argues in favor of the H_4B site to recognize a fully protonated pterin. The stabilization of the pterin radical does not stem from the protonation, per se, but from the ability to restrict the lone pair on N-5 of the pterin ring (Kappock and Caradonna, 1996). Cycling between the pterin radical and H_4B may be achieved via electron transfer from the reductase domain while the pterin remains bound to NOS. The results have already alluded to the possibility of docking the reductase (FMN) domain in the vicinity of the zinc center and pterin site, which could facilitate the one-electron reduction of the pterin radical to H_4B. Based on rapid reaction kinetics, a pterin radical has been proposed in nNOS (Bec et al., 1998), and the eNOS heme domain structure lends mechanistic support for its involvement in the catalysis. Also, evidence for a protein-bound pterin radical species in aldehyde dehydrogenase was recently provided via EPR spectroscopy (Luykx et al., 1998). Further, aromatic stacking is not a common feature in binding sites of other pterin-utilizing enzymes (Auerbach et al., 1997; with the exception of TS and ricin), but resonance stabilization of the semiquinone radical found in flavoproteins are mediated through stacking interactions. The cation–π interactions are strong and specific (Dougherty, 1996), and H_4B cation-π interactions with W449 and F462 may play a key role in the molecular recognition of pterin by eNOS. NOS provides an example where an enzyme may have evolved to accommodate a pterin function to mimic flavoprotein systems in structure and mechanism.

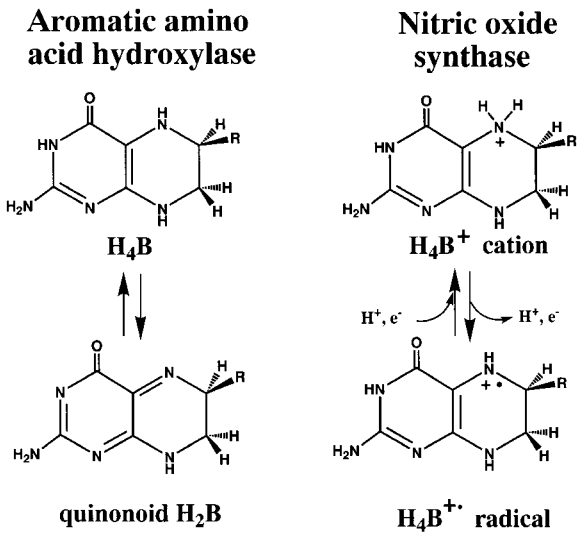

Figure 7. Proposed Mechanism for Pterin in NO Biosynthesis

The uniqueness of the H_4B–eNOS interaction (Figure 4) and the ability to bind L-Arg at the pterin site present a strong case for the involvement of a pterin radical in NOS catalysis and rule out the possibility of $H_4B \leftrightarrow qH_2B$ cycling during NO biosynthesis. R represents the dihydroxypropyl side chain at the C6 position on the pterin ring.

Experimental Procedures

Expression, Purification, and Crystallization of eNOS Heme Domain

Bovine eNOS heme domain (39–482; Mr 49,000) was obtained via trypsinolysis of a holo eNOS construct missing 75% of the calmodulin-binding region. The expression of eNOS in *Escherichia coli* and protein purification methods have been described previously (Martásek et al., 1996). Crystals suitable for diffraction were grown by the sitting drop vapor-diffusion method from 15% PEG 3350, 200 mM magnesium acetate, 100 mM sodium cacodylate (pH 6.5), and 1 mM SEITU (or 5 mM L-Arg) in the presence of 35 μM sodium dodecyl sulfate (SDS) as an additive and 5 mM Tris(2-carboxyethyl)phosphine (TCEP) or 5 mM glutathione sulfonate as reducing agent. Crystals grown under these conditions belong to the orthorhombic space group, $P2_12_12_1$, with cell constants a = 58.00 Å, b = 106.55 Å, and c = 156.22 Å. There is one dimer in the asymmetric unit (50% solvent content). All native and derivative crystals were flash frozen in liquid nitrogen for both storage and data collection at cryogenic temperatures (100 K). A protein stabilization cocktail containing 15% glycerol, 11% trehalose, 8% mannitol, and 8% sucrose was used as cryoprotectant.

Structure Determination and Refinement

Table 1 provides a summary of data collection statistics, phase determination, and structure refinement. Data were collected with a charge coupled device (CCD) detector at ALS, CHESS, NSLS, and SSRL (beamlines 5.0.2, F1 and F2, X12B, and 1–5, respectively) and with a Mar Research image plate scanner at SSRL (beamlines 7–1

Table 1. Data Collection, Phasing, and Refinement Statistics

Data Collection

	+H_4B, +SEITU	−H_4B, +SEITU	−H_4B, +Arg	Se-edge	Se-peak	Se-remote	Se-EMP[a]	Se-$OsO_3(Py)_2$[a]
Wavelength (Å)	0.9798	1.08	1.000	0.9801	0.9794	0.9252	1.08	1.08
Resolution limits (Å)	1.9	2.1	1.95	2.3	2.3	2.3	2.3	3.0
Total observations	217,080	204,608	255,850	131,275	127,968	144,570	131,287	74,034
Unique observations	74,337	57,723	69,580	40,100	36,351	40,965	40,508	16,204
R_{sym}	0.044	0.084	0.054	0.048	0.054	0.044	0.059	0.085
R_{sym} (outer shell)	0.175	0.563	0.660	0.121	0.219	0.185	0.325	0.336
$<I/\sigma>$	19.3	7.7	9.6	16.9	15.3	17.1	9.8	8.9
$<I/\sigma>$ (outer shell)	3.5	2.4	1.6	3.2	2.2	3.1	2.2	4.0
Completeness	0.965	0.996	0.983	0.962	0.988	0.985	0.977	0.808
Completeness (outer shell)	0.800	0.996	0.983	0.795	0.802	0.983	0.801	0.829
MAD phasing (20.0–2.35 Å)								
No. of sites				6				
Phasing power Iso/Ano				0.0/0.76	0.0/0.78	1.1/0.75		
R_{cullis} Iso/Ano				0.0/0.96	0.97/0.96	0.41/0.95		
MIRAS phasing								
No. of sites							6	5
R_{iso}							0.157	0.173
R_{cullis}							0.89	0.92
Phasing power Iso/Ano							1.15/0.87	0.71/0.85
Overall FOM (MAD+MIRAS)				0.29 (2.35 Å)				

Refinement

	Resolution (Å)	Protein Atoms	Waters	R Factor	R_{free}	Reflections	Rms Deviation[b]
X-PLOR (+H_4B,+SEITU)	30.0–1.9	6593	591	0.225 (F>2σF)	0.262	73,483 (F>2σF)	
SHELXL (+H_4B, +SEITU)	10.0–1.9	6593	591	0.207	0.278	70,029	0.007 Å, 0.021 Å
X-PLOR (−H_4B, +SEITU)	30.0–2.1	6593	336	0.197 (F>2σF)	0.252	48,347 (F>2σF)	0.007 Å, 1.408°
X-PLOR (−H_4B, +Arg)	30.0–1.95	6593	402	0.212 (F>2σF)	0.260	56,572 (F>2σF)	0.008 Å, 1.473°

$R_{sym} = \Sigma|I - <I>|/\Sigma I$, where I is the observed intensity and $<I>$ the average intensity of multiple symmetry-related observations of that reflection. $R_{iso} = \Sigma|F_{PH} - F_P|/\Sigma F_P$. R_{cullis} Iso (acentric) = rms lack of closure/rms isomorphous difference (statistics from SHARP). R_{cullis} Ano = rms lack of closure/rms anomalous difference (statistics from SHARP). Phasing power = rms heavy atom structure factor/phase-integrated lack of closure (statistics from SHARP). Overall FOM, overall figure of merit (from SHARP). R_{free} = R factor calculated using 5% (3685 reflections) of the reflection data chosen randomly and set aside from the start of the refinement.

[a] EMP, ethyl mercuric phosphate. OsO_3Py_2, osmium bis-pyridine; heavy atom derivatives were prepared with crystals generated by cocrystallization with the Se inhibitor.

[b] Rms deviations are defined as bond length and angular distances in SHELXL and bond length and bond angle, respectively, in X-PLOR. (+H_4B, +SEITU), structure with H_4B bound at the pterin site and SEITU bound at the active site; (−H_4B, +SEITU), H_4B-free structure with L-Arg bound at the pterin site and SEITU bound at the active site; (−H_4B, +Arg), H_4B-free structure with L-Arg bound at the active site; Se-edge, structure with H_4B bound at the pterin site and L-Arg bound at the active site.

and 9–1). Multiwavelength anomalous diffraction (MAD) data were collected at three wavelengths near the Se absorption edge using the inverse beam mode after aligning the crystal with a major axis coincident with the rotation axis so that Bijvoet pairs could be measured simultaneously. Image plate data were reduced using the programs DENZO and SCALEPACK (Otwinoski and Minor, 1997), and CCD data were processed with the DPS (Steller et al., 1997), MOSFLM, and CCP4 suite of programs (Collaborative Computational Project No. 4, 1994). Mercury and osmium positions (three sites each) were readily identified by SHELXS (Sheldrick, 1997) and could later be confirmed in the isomorphous and anomalous difference Patterson maps. Iterative rounds of rejections performed with ENDHKL (Louis Sanchez, Cal. Tech.) in conjunction with SCALEPACK (Otwinoski and Minor, 1997) and local scaling were both critical for the identification of the heavy atoms. For MAD phasing an inhibitor, S-(2-(5((amidinothio)methyl)-2-thienyl)ethyl)isothiourea (Garvey et al., 1994), was prepared with the sulfur atoms replaced with selenium. Once the structure was refined, it was evident that the inhibitor had not bound. Three out of six sites initially assigned to selenium were the new zinc site and two arsenic sites. Both atom types, Zn and As, were confirmed via a thorough analysis of Bijovet difference Fourier calculations at multiple wavelengths. Two of the six sites initially assigned to selenium are most likely adducts of $(CH_3)_2$As to both Cys-384 residues (one per monomer) from the cacodylate buffer used in crystallization. Since the crystallization solution contains excess reducing agents, we attribute this chemistry (Barber, 1932) to the reduction of dimethylarsinate (V) to dimethylarsonite (III) followed by reaction with Cys-384. The three remaining sites initially thought to be selenium, two near both Cys-214 sulfurs and one near Cys-87, were much weaker and could not be confidently modeled as $(CH_3)_2$As sites in the final refined electron density map. Despite the incorrect assignment of the arsenic and zinc sites as selenium, their inclusion was essential for obtaining an interpretable electron density map. Availability of heme iron positions, identified independently via anomalous scattering at the Fe edge, greatly facilitated the location of heavy atom sites. Heavy atom derivative screening was carried out with PHASES (Furey and Swaminathan, 1997) and visualized using XTALVIEW (McRee, 1993). The final combined MAD and heavy atom refinement was done with SHARP (de La Fortelle and Bricogne, 1997) followed by density modification with either SOLOMON (Abrahams and Leslie, 1996) or DM. The latter calculation includes noncrystallographic symmetry (NCS) averaging. The resulting experimental MAD-heavy atom derivative map at 2.35 Å was of sufficient quality to allow nearly all the

main chain atoms and 80% of the side chain atoms to be built into the model before the first round of refinement. Phase refinement with heavy atom data alone did not produce an interpretable map. Heme iron positions, SHELXS, MAD phasing, SHARP, and synchrotron radiation were a sine qua non for success in the structure solution. Structural refinement was performed with XPLOR (Brünger, 1992) and SHELXL (Sheldrick and Schneider, 1997). Five percent of the data were set aside for free-R cross validation prior to any structural refinement. The protein model was built using TOM and improved with SigmaA-weighted $2|F_{obs}| - |F_{calc}|$ and $|F_{obs}| - |F_{calc}|$ maps iteratively with X-PLOR refinement. A bulk solvent correction was used in the final stages of the X-PLOR but not in the SHELXL refinement. The current model at 1.9 Å resolution includes 830 residues (residues 67–482 in molecule A; 69–482 in molecule B) and 591 waters. Residues 39–66 and 108–121 are disordered primarily due to the proline-rich nature of these regions. Ramachandran plots generated with PROCHECK showed that 90.2% of the residues were in the most favored regions and 9.6% were in additional allowed regions. Solvent-accessible surface area calculations were done with MSP (Connolly, 1993).

Acknowledgments

C. S. R. is delighted to acknowledge W. Lipscomb and B. Vallee for stimulating dialogs on zinc; E. de La Fortelle for constructive suggestions regarding SHARP phasing; C. Nielsen and X-P. Dai for help with CCD data processing; L. Sanchez for ENDHKL; T. Terwilliger for SOLVE; S. Islam for PREPI; A. Greenwood for help with graphics; M. Connolly for MSP; S. Jain, T. Rydel, D. Schuller, W. Sessa, I. Sevrioukova, and S. Veeraraghavan for helpful discussions; M. Sundaramoorthy for stimulating discussions and help with SHELXL refinement; G. Petsko for EMP; and R. Stevens for generously providing coordinates of pterin-bound TyrOH before publication. We are grateful to A. McPherson for the use of his laboratory facilities and advice. We would like to thank the following synchrotron sources for timely access to their beamlines and their staffs for help with data collection: ALS (T. Earnest and L-W. Hung, 5.0.2); CHESS (A. Deacon, D. Thiel and staffs of F-1 and F-2); NSLS (M. Capel, X12B); and SSRL (H. Bellamy, 1-5; A. Cohen, P. Ellis, P. Kuhn, H-D. Nuhn, and M. Soltis, 7-1 and 9-1). This work was supported by the National Institutes of Health (grants GM32688 and GM57353 to T. L. P.; HL30050 and GM52419 to B. S. S. M.), the Robert A. Welch Foundation (grant AQ-1192 to B. S. S. M.), the Ministry of Education of Czech Republic (V. K.), the Howard Hughes Medical Institute (V. K.), and Berlex Corp. (T. L. P.). C. S. R. is a Fellow of the American Heart Association (Western States Affiliate) and is grateful for their support of this work.

Received September 28, 1998; revised November 9, 1998.

References

Abrahams, J.P., and Leslie, A.G.W. (1996). Methods used in the structure determination of bovine mitochondrial F-1 ATPase. Acta Crystallogr. *D52*, 30–42.

Alderton, W.K., Boyhan, A., and Lowe, P.N. (1998). Nitroarginine and tetrahydrobiopterin binding to the haem domain of neuronal nitric oxide synthase using a scintillation proximity assay. Biochem. J. *332*, 195–201.

Auerbach, G., Herrmann, A., Gutlich, M., Fischer, M., Jacob, U., Bacher, A., and Huber, R. (1997). The 1.25 Å crystal structure of sepiapterin reductase reveals its binding mode to pterins and brain neurotransmitters. EMBO J. *16*, 7219–7230.

Barber, H.J. (1932). The hydrolysis of arylthioarsinites. J. Chem. Soc. 1365–1368.

Bec, N., Gorren, A.C., Voelker, C., Mayer, B., and Lange, R. (1998). Reaction of neuronal nitric-oxide synthase with oxygen at low temperature. Evidence for reductive activation of the oxy-ferrous complex by tetrahydrobiopterin. J. Biol. Chem. *273*, 13502–13508.

Berry, M.B., and Phillips, G.N., Jr. (1998). Crystal structures of *Bacillus stearothermophilus* adenylate kinase with bound Ap5A. Proteins *32*, 276–288.

Birdsall, D.L., Finer-Moore, J., and Stroud, R.M. (1996). Entropy in bisubstrate enzymes: proposed role of an alternate site in chaperoning substrate into, and products out of, thymidylate synthase. J. Mol. Biol. *255*, 522–535.

Bourne, H.R., Sanders, D.A., and McCormick, F. (1991). The GTPase superfamily: conserved structure and molecular mechanism. Nature *349*, 117–127.

Brünger, A.T. (1992). X-PLOR version 3.1: a system for X-ray crystallography and NMR. (New Haven, CT: Yale University Press).

Collaborative Computational Project, Number 4. (1994). The CCP4 suite: programs for protein crystallography. Acta Crystallogr. *D50*, 760–763.

Chan, M.K., Mukund, S., Kletzin, A., Adams, M.W., and Rees, D.C. (1995). Structure of a hyperthermophilic tungstopterin enzyme, aldehyde ferredoxin oxidoreductase. Science *267*, 1463–1469.

Chen, P-F., Tsai, A-L., and Wu, K.K. (1995). Cysteine 99 of endothelial nitric oxide synthase (NOS-III) is critical for tetrahydrobiopterin-dependent NOS-III stability and activity. Biochem. Biophys. Res. Commun. *215*, 1119–1129.

Connolly, M.L. (1993). The molecular surface package. J. Mol. Graph. *11*, 139–143.

Cosentino, F., Patton, S., d'Uscio, L.V., Werner, E.R., Werner-Felmayer, G., Moreau, P., Malinski, T., and Lüscher, T.F. (1998). Tetrahydrobiopterin alters superoxide and nitric oxide release in prehypertensive rats. J. Clin. Invest. *101*, 1530–1537.

Couet, J., Li, S., Okamoto, T., Ikezu, T., and Lisanti, M.P. (1997). Identification of peptide and protein ligands for the caveolin-scaffolding domain. Implications for the interaction of caveolin with caveolae-associated proteins. J. Biol. Chem. *272*, 6525–6533.

Crane, B.R., Arvai, A.S., Gachhui, R., Wu, C.Q., Ghosh, D.K., Getzoff, E.D., Stuehr, D.J., and Tainer, J.A. (1997). The structure of nitric oxide synthase oxygenase domain and inhibitor complexes. Science *278*, 425–431.

Crane, B.R., Arvai, A.S., Ghosh, D.K., Wu, C.Q., Getzoff, E.D., Stuehr, D.J., and Tainer, J.A. (1998). Structure of nitric oxide synthase oxygenase dimer with pterin and substrate. Science *279*, 2121–2126.

Cronk, J.D., Endrizzi, J.A., and Alber, T. (1996). High-resolution structures of the bifunctional enzyme and transcriptional coactivator DCoH and its complex with a product analogue. Prot. Sci. *5*, 1963–1972.

Crow, J.P., Sampson, J.B., Zhuang, Y., Thompson, J.A., and Beckman, J.S. (1997). Decreased zinc affinity of amyotrophic lateral sclerosis-associated superoxide dismutase mutants leads to enhanced catalysis of tyrosine nitration by peroxynitrite. J. Neurochem. *69*, 1936–1944.

de La Fortelle, E., and Bricogne, G. (1997). Maximum-likelihood heavy atom parameter refinement for multiple isomorphous replacement and multiwavelength anomalous diffraction methods. Methods Enzymol. *276*, 472–494.

Dinerman, J.L., Lowenstein, C.J., and Snyder, S.H. (1993). Molecular mechanisms of nitric oxide regulation. Potential relevance to cardiovascular disease. Circ. Res. *73*, 217–222.

Dougherty, D.A. (1996). Cation-pi interactions in chemistry and biology: a new view of benzene, Phe, Tyr and Trp. Science *271*, 163–168.

Furey, W., and Swaminathan, S. (1997). PHASES-95: a program for the processing and analysis of diffraction data from macromolecules. Methods Enzymol. *277*, 590–620.

García-Cardeña, G., Martásek, P., Masters, B.S.S., Skidd, P.M., Couet, J., Li, S., Lisanti, M.P., and Sessa W.C. (1997). Dissecting the interaction between nitric oxide synthase (NOS) and caveolin. Functional significance of the NOS caveolin binding domain in vivo. J. Biol. Chem. *272*, 25437–25440.

Garvey, E.P., Oplinger, J.A., Tanoury, G.J., Sherman, P.A., Fowler, M., Marshall, S., Harmon, M.F., Paith, J.E., and Furfine, E.S. (1994). Potent and selective inhibition of human nitric oxide synthases. Inhibition by non-amino acid isothioureas. J. Biol. Chem. *269*, 26669–26676.

Gatti, D.L., Palfey, B.A., Lah, M.S., Entsch, B., Massey, V., Ballou, D. P., and Ludwig, M.L. (1994). The mobile flavin of 4-OH benzoate hydroxylase. Science *266*, 110–114.

Gergel, D., and Cederbaum, A.I. (1996). Inhibition of the catalytic activity of alcohol dehydrogenase by nitric oxide is associated with S-nitrosylation and the release of zinc. Biochemistry *35*, 16186–16194.

Ghosh, D.K., Wu, C.Q., Pitters, E., Moloney, M., Werner, E.R., Mayer, B., and Stuehr, D.J. (1997). Characterization of the inducible nitric oxide synthase oxygenase domain identifies a 49 amino acid segment required for subunit dimerization and tetrahydrobiopterin interaction. Biochemistry *36*, 10609–10619.

Goodwill, K.F., Sabatier, C., and Stevens, R.C. (1998). Crystal structure of tyrosine hydroxylase with bound cofactor analogue and iron at 2.3 Å resolution: self hydroxylation of Phe300 and the pterin-binding site. Biochemistry *37*, 13437–13445.

Griffith, O.W., and Stuehr, D.J. (1995). Nitric oxide synthases: properties and catalytic mechanism. Annu. Rev. Physiol. *57*, 707–736.

Hampele, I.C., D'Arcy, A., Dale, G.E., Kostrewa, D., Nielsen, J., Oefner, C., Page, M.G., Schonfeld,H. J., Stuber, D., and Then, R.L. (1997). Structure and function of the dihydropteroate synthase from *Staphylococcus aureus*. J. Mol. Biol. *268*, 21–30.

Hecker, M., Sessa, W.C., Harris, H.J., Anggard, E.E., and Vane, J.R. (1992). The metabolism of L-arginine and its significance for the biosynthesis of endothelium-derived relaxing factor: cultured endothelial cells recycle L-citrulline to L-arginine. Proc. Natl. Acad. Sci. USA *87*, 8612–8616.

Hemmens, B., and Mayer, B. (1997). Enzymology of nitric oxide synthases. Methods Mol. Biol. *100*, 1–32.

Hennig, M., D'Arcy, A., Hampele, I.C., Page, M.G.P., Oefner, C., and Dale, G.E. (1998). Crystal structure and reaction mechanism of 7,8-dihydroneopterin aldolase from *Staphylococcus aureus*. Nature Struct. Biol. *5*, 357–362.

Huang, Z., Huang, P.L., Panahian, N., Dalkara, T., Fishman, M.C., and Moskowitz, M.A. (1994). Effects of cerebral ischemia in mice deficient in neuronal nitric oxide synthase. Science *265*, 1883–1885.

Hyun, J., Komori, Y., Chaudhuri, G., Ignarro, L.J., and Fukuto, J.M. (1995). The protective effect of tetrahydrobiopterin on the nitric oxide-mediated inhibition of purified nitric oxide synthase. Biochem. Biophys. Res. Commun. *206*, 380–386.

Kappock, T.J., and Caradonna, J.P. (1996). Pterin dependent amino acid hydroxylases. Chem. Rev. *96*, 2659–2756.

Kaufman, S. (1997). Tetrahydrobiopterin: Basic Biochemistry and Role in Human Disease. (Baltimore, MD: Johns Hopkins University Press).

Knowles, R.G., and Moncada, S. (1994). Nitric oxide synthases in mammals. Biochem. J. *298*, 249–258.

Kwon, N.S., Nathan, C.F., and Stuehr, D.J. (1989). Reduced biopterin as a cofactor in the generation of nitrogen oxides by murine macrophages. J. Biol. Chem. *264*, 20496–20501.

Lipscomb, W.N., and Sträter, N. (1996). Recent advances in zinc enzymology. Chem. Rev. *96*, 2375–2433.

Luykx, D.M., Duine, J.A., and de Vries, S. (1998). Molybdopterin radical in bacterial aldehyde dehydrogenase. Biochemistry *37*, 11366–11375.

Maret, W., and Vallee, B.L. (1998). Thiolate ligands in metallothionein confer redox activity on zinc clusters. Proc. Natl. Acad. Sci. USA *95*, 3478–3482.

Marletta, M. (1994). Nitric oxide synthase: aspects concerning structure and catalysis. Cell *78*, 927–930.

Martásek, P., Liu, Q., Liu, J., Roman, L.J., Gross, S.S., Sessa, W.C., and Masters, B.S.S. (1996). Characterization of bovine endothelial nitric oxide synthase expressed in E. coli. Biochem. Biophys. Res. Commun. *219*, 359–365.

Masters, B.S.S., McMillan, K., Sheta, E.A., Nishimura, J.S., Roman, L.J., and Martásek P. (1996). Neuronal nitric oxide synthase, a modular enzyme formed by convergent evolution: structure studies of a cysteine thiolate-liganded heme protein that hydroxylates L-arginine to produce NO· as a cellular signal. FASEB J. *10*, 552–558.

Matthews, R.G. (1982). Are the redox properties of tetrahydrofolate cofactors utilized in folate-dependent reactions? Fed. Proc. *41*, 2600–2604.

McRee, D.E. (1993). Practical Protein Crystallography. (New York, NY: Academic Press).

McTigue, M.A., Davies, J.F., Kaufman, B.T., and Kraut, J. (1993). Crystal structures of chicken liver dihydrofolate reductase: binary thioNADP+ and ternary thioNADP+·biopterin complexes. Biochemistry *32*, 6855–6862.

Miller, R.T., Martásek, P., Roman, L.J., Nishimura, J.S., and Masters, B.S.S. (1997). Involvement of the reductase domain of neuronal nitric oxide synthase in superoxide anion production. Biochemistry *36*, 15277–15284.

Nathan, C. (1995). Natural resistance and nitric oxide. Cell *82*, 873–876.

Nicholls, A., Bharadwaj, R., and Honig, B. (1993). GRASP: graphical representation and analysis of surface properties. Biophys. J. *64*, 166–170.

Otwinowski, Z., and Minor, W. (1997). Processing of X-ray diffraction data collected in oscillation mode. Methods Enzymol. *276*, 307–326.

Perry, J.M., and Marletta, M.A. (1998). Effects of transition metals on nitric oxide synthase catalysis. Proc. Natl. Acad. Sci. USA *95*, 11101–11106.

Pollock, J.S., Förstermann, U., Mitchell, J.A., Warner, T.D., Schmidt, H.H., Nakane, M., and Murad, F. (1991). Purification and characterization of particulate endothelium-derived relaxing factor synthase from cultured and native bovine aortic endothelial cells. Proc. Natl. Acad. Sci. USA *88*, 10480–10484.

Presta, A., Siddhanta, U., Wu, C., Sennequier, N., Huang, L., Abu-Soud, H.M., Erzurum, S., and Stuehr, D.J. (1998). Comparative functioning of dihydro- and tetrahydropterins in supporting electron transfer, catalysis, and subunit dimerization in inducible nitric oxide synthase. Biochemistry *37*, 298–310.

Rodríguez-Crespo, I., Moënne-Loccoz, P., Loehr, T.M., and Ortiz de Montellano, P.R. (1997). Endothelial nitric oxide synthase: modulations of the distal heme site produced by progressive N-terminal deletions. Biochemistry *36*, 8530–8538.

Roman, L.J., Sheta, E.A., Martásek, P., Gross, S.S., Liu, Q., and Masters, B.S.S. (1995). High-level expression of functional rat neuronal nitric oxide synthase in Escherichia coli. Proc. Natl. Acad. Sci. USA *92*, 8428–8432.

Schmeichel, K.L., and Beckerle, M.C. (1994). The LIM domain is a modular protein-binding interface. Cell *79*, 211–219.

Schwabe, J.W., and Klug, A. (1994). Zinc mining for protein domains. Nature Struct. Biol. *1*, 345–349.

Shaul, P.W., Smart, E.J., Robinson, L.J., German, Z., Yuhanna, I.S., Ying, Y., Anderson, R.G., and Michel, T. (1996). Acylation targets endothelial nitric-oxide synthase to plasmalemmal caveolae. J. Biol. Chem. *271*, 6518–6522.

Sheldrick, G.M. (1997). Patterson superposition and ab initio phasing. Methods Enzymol. *276*, 628–641.

Sheldrick, G.M., and Schneider, T.R. (1997). SHELXL: high resolution refinement. Methods Enzymol. *277*, 319–343.

Stamler, J.S. (1994). Redox signaling: nitrosylation and related target interactions of nitric oxide. Cell *78*, 931–936.

Steller, I., Bolotovsky, R., and Rossman, M.G. (1997). An algorithm for automatic indexing of oscillation images using Fourier analysis. J. Appl. Crystallogr. *30*, 1036–1040.

Stroes, E., Kastelein, J., Cosentino, F., Erkelens, W., Wever, R., Koomans, H., Lüscher, T., and Rabelink, T. (1997). Tetrahydrobiopterin restores endothelial function in hypercholesterolemia. J. Clin. Invest. *99*, 41–46.

Tayeh, M.A., and Marletta, M.A. (1989). Macrophage oxidation of L-arginine to nitric oxide, nitrite, and nitrate: tetrahydrobiopterin is required as a cofactor. J. Biol. Chem. *264*, 19654–19658.

Tsukihara, T., Aoyama, H., Yamashita, E., Tomizaki, T., Yamaguchi, H., Shinzawa-Itoh, K., Nakashima, R., Yaono, R., and Yoshikawa, S. (1995). Structures of metal sites of oxidized bovine heart cytochrome c oxidase at 2.8 Å. Science *269*, 1069–1074.

Vallee, B.L., and Auld, D.S. (1993). Zinc: biological functions and coordination motifs. Acc. Chem. Res. *26*, 543–551.

Varughese, K.I., Skinner, M.M., Whiteley, J.M., Matthews, D.A., and

Xuong, N.H. (1992). Crystal structure of rat liver dihydropteridine reductase. Proc. Natl. Acad. Sci. USA *89*, 6080–6084.

Vásquez-Vivar, J., Kalyanaraman, B., Martásek, P., Hogg, N., Masters, B.S.S., Karoui, H., Tordo, P., and Pritchard, K.A., Jr. (1998). Superoxide generation by endothelial nitric oxide synthase. The influence of cofactors. Proc. Natl. Acad. Sci. USA *95*, 9220–9225.

Venema, R.C., Ju, H., Zou, R., Ryan, J.W., and Venema, V.J. (1997). Subunit interactions of endothelial nitric oxide synthase. J. Biol. Chem. *272*, 1276–1282.

Wang, M., Roberts, D.L., Paschke, R., Shea, T.M., Masters, B.S.S., and Kim, J.J. (1997). Three-dimensional structure of NADPH-cytochrome P450 reductase: prototype for FMN- and FAD-containing enzymes. Proc. Natl. Acad. Sci. USA *94*, 8411–8416.

Werner-Felmayer, G., and Gross, S.S. (1996). Analysis of tetrahydrobiopterin and its role in nitric oxide synthesis. In Methods in Nitric Oxide Research, M. Feelisch and J.S. Stamler, eds (New York: John Wiley and Sons), pp. 271–299.

Wilker, J.J., and Lippard, S.J. (1995). Modelling the DNA-methylphosphotriester repair site in *Escherichia coli* ADA. Why zinc and four cysteines? J. Am. Chem. Soc. *117*, 8682–8683.

Witteveen, C., Giovanelli, J., and Kaufman, S. (1996). Reduction of quinonoid dihydrobiopterin to tetrahydrobiopterin by nitric oxide synthase. J. Biol. Chem. *271*, 4143–4147.

Yan, X., Hollis, T., Svinth, M., Day, P., Monzingo, A.F., Milne, G.W.A., and Robertus, J.D. (1997). Structure-based identification of a ricin inhibitor. J. Mol. Biol. *266*, 1043–1049.

Yarus, M. (1988). A specific amino acid binding site composed of RNA. Science *240*, 1751–1758.

Yu, H.T., and Schreiber, S.L. (1996). Structure of guanine-nucleotide-exchange factor human Mss4 and identification of its Rab-interacting surface. Nature *376*, 788–791.

Brookhaven Protein Data Bank ID Codes

Coordinates have been deposited with the ID codes 1NSE, 2NSE, 3NSE, and 4NSE.